Nanoscopic Assessment of Anti-SARS-CoV-2 Spike Neutralizing Antibody Using High-Speed AFM

Keesiang Lim,* Goro Nishide, Elma Sakinatus Sajidah, Tomoyoshi Yamano, Yujia Qiu, Takeshi Yoshida, Akiko Kobayashi, Masaharu Hazawa, Toshio Ando, Rikinari Hanayama,* and Richard W. Wong*

Cite This: Nano Lett. 2023, 23, 619−628

Read Online

ACCESS | Metrics & More | Article Recommendations | Supporting Information

ABSTRACT: Anti-spike neutralizing antibodies (S NAbs) have been developed for prevention and treatment against COVID-19. The nanoscopic characterization of the dynamic interaction between spike proteins and S NAbs remains difficult. By using high-speed atomic force microscopy (HS-AFM), we elucidate the molecular property of an S NAb and its interaction with spike proteins. The S NAb appeared as monomers with a Y conformation at low density and formed hexameric oligomers at high density. The dynamic S NAb−spike protein interaction at RBD induces neither RBD opening nor S1 subunit shedding. Furthermore, the interaction was stable at endosomal pH. These findings indicated that the S NAb could have a negligible risk of antibody-dependent enhancement.

Dynamic movement of spike proteins on small extracellular vesicles (S sEV) resembled that on SARS-CoV-2. The sensitivity of variant S sEVs to S NAb could be evaluated using HS-AFM. Altogether, we demonstrate a nanoscopic assessment platform for evaluating the binding property of S NAbs.

KEYWORDS: SARS-CoV-2 spike protein, SARS-CoV-2 spike nanoparticle, receptor-binding domain, antispike neutralizing antibody, antibody-dependent enhancement, high-speed atomic force microscopy, nanoimaging
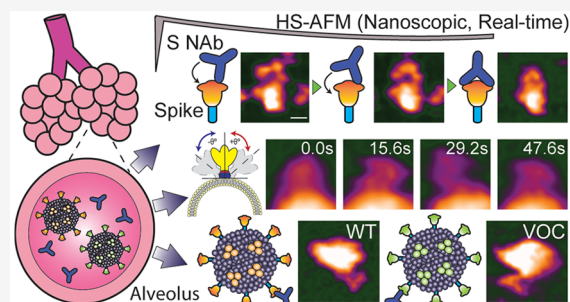
M ore than 500 million cases of coronavirus disease 2019 (COVID-19) have been registered worldwide.[1] Severe acute respiratory syndrome coronavirus 2 (SARS-CoV-2) suppresses the host immune response to make infected people asymptomatic (reviewed in ref 2), and this promotes mass infection that drives the virus to evolve rapidly. The spike (S) protein of SARS-CoV-2 not only mediates viral entry but also triggers the host immune response to produce anti-spike neutralizing antibodies (S NAbs). Therefore, because of selection pressure, alterations within S proteins of SARS-CoV-2 variants frequently occur, predominantly in the receptor-binding domain (RBD) and the N-terminal domain (NTD). For example, alterations in the RBD (K417N, L452R, and T478 K) and NTD (T19R, G142D, Del 156−157, R158G) of the Delta variant (B.1.617.2) enhance viral transmissibility and promote immune escape (reviewed in ref 3). The Delta variant has greater resistance than the Alpha variant (B.1.1.7) to the Pfizer/BioNTech BNT162b2 mRNA vaccine (88% vs 93.7%).[4] COVID-19 mRNA vaccines (BNT162b2 and Moderna mRNA-1273) take 2−4 weeks to confer peak immunity;[5] however, the durability of protection only lasts 1−8 months after the second dose.[5,6] As a result, multiple booster doses of COVID-19 mRNA vaccine are required to protect effectively against COVID-19.

Now, S NAbs specific to RBD or NTD can be identified via high-throughput screening of antigen-specific B cells isolated from convalescent COVID-19 patients (review in ref 7). In addition to COVID-19 mRNA vaccines, these S NAbs could rapidly provide passive immunity for prevention and treatment against COVID-19 (review in ref 7). Conceptually, S NAbs prevent SARS-CoV-2 entry by blocking S protein interaction with its receptor, the angiotensin-converting enzyme 2 (ACE2). Nonetheless, some S NAbs exhibit antibody-dependent enhancement (ADE) by promoting S1 subunit shedding after the antibodies bind to all three RBDs.[8] S1 subunit shedding exposes the S2 subunit for proteolytic cleavage of the S2′ site to initiate membrane fusion.[9] These findings imply that real-time observations of dynamic S NAb−S protein interactions at a nanoscopic level could be essential to evaluate the ADE risk. Unfortunately, the temporal resolution of cryo-EM is insufficient to achieve this goal. Furthermore, interactions between Fab fragments and S proteins in cryo-EM imaging often ignore the importance of antibody bivalency and the Fc region. The whole antibody (IgG1) and Fab fragment demonstrate different outcomes in both S protein
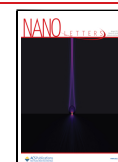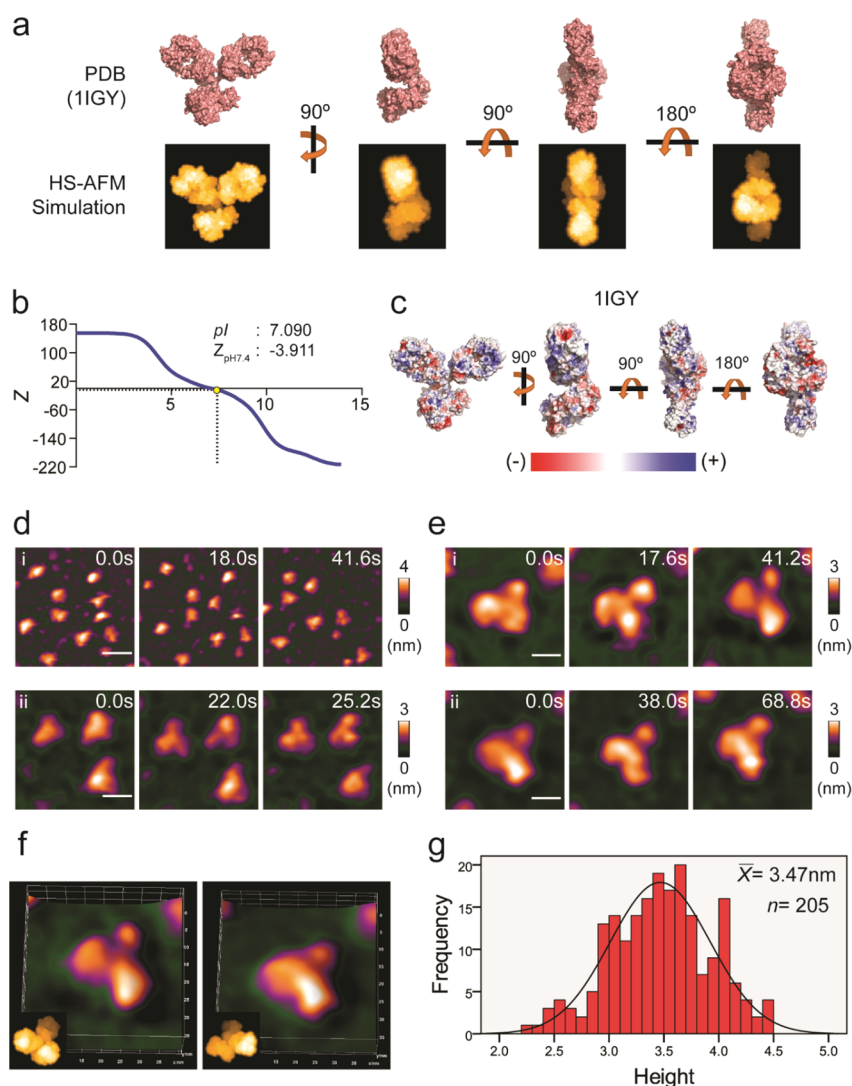
Figure 1. Molecular properties and nanotopology of anti-severe acute respiratory syndrome coronavirus 2 (SARS-CoV-2) spike neutralizing antibody MM43. (a) Simulated high-speed atomic force microscopy (HS-AFM) images, using the X-ray crystallographic structure of IgG1 (PDB: 1IGY) as a template. (b) Net charge (Z) of IgG1 as a function of pH (pI, isoelectric point; $Z_{pH7.4}$, ζ potential at pH 7.4). (c) Surface charge map of IgG1 at pH 7.4, generated using PDB 2PQR and APBS analysis. (d, e) Two representative HS-AFM image sequences of MM43 in a group (d) and single (e). These images are taken from Movie S1 (n_{group}, n_{single} = 10; scale bars: (d-i) 40 nm- , (d-ii) 15 nm, (e-i,ii) 10 nm). (f) 3D surface plots of MM43 in different orientations. (g) Histogram and a Gaussian fit of the MM43 height distribution.

neutralizing and enhancing antibodies. For example, Asarnow et al. reported that the whole 5A6 antibody but not its Fab fragment prevented cell syncytium formation.[8] In contrast, Liu et al. found that the bivalent binding of NTD-specific antibody promotes RBD opening and hence it enhances SARS-CoV-2 infection.[10] Besides the antibody–antigen interaction, nanoscopic observation of dynamic interactions between S NAb and SARS-CoV-2 virus could reflect the accessibility to S protein on viral surface by S NAb.

High-speed atomic force microscopy (HS-AFM) is a powerful nanoimaging tool with high spatiotemporal resolution. We have demonstrated that HS-AFM is suitable for real-time visualization of the conformational dynamics of viral fusion proteins,[11−13] histone H2A−DNA interactions,[14] and organelles such as nuclear pore complexes,[15,16] and small extracellular vesicles (sEVs)[12,13] at a nanoscale level. In this study, we used HS-AFM to develop a nanoscopic assessment platform to determine the binding property of an S NAb (MM43) and ADE risk by observing the interaction between

MM43 and S protein. Additionally, we conducted the real-time visualization of the MM43 interaction with S protein-expressing sEV (S sEV) to mimic the scenario of SARS-CoV-2 neutralization.

Most of the Food and Drug Administration (FDA) and European Medicine Agency (EMA) approved therapeutic S NAbs for COVID-19 treatment are subclass IgG1 (reviewed in ref 17). Hence, we first performed nanoimaging of an S NAb (mouse IgG1, catalogue number 40591-MM43) using HS-AFM to study the native conformation and conformational dynamics of IgG1. Before HS-AFM scanning, we simulated a mouse IgG1 crystal structure (PDB: 1IGY) to its HS-AFM images (Figure 1a) by using the bioAFMviewer software.[18] To determine a suitable substrate for MM43 adsorption, the net surface charge of IgG1 at pH 7.4 was computed using the Protein Tool on the Prot Pi Web site (Figure 1b). Additionally, a surface electrostatic map of IgG1 at neutral pH was generated by performing PDB 2PQR[19] and APBS[20] analysis (Figure 1c). The results suggested that bare mica
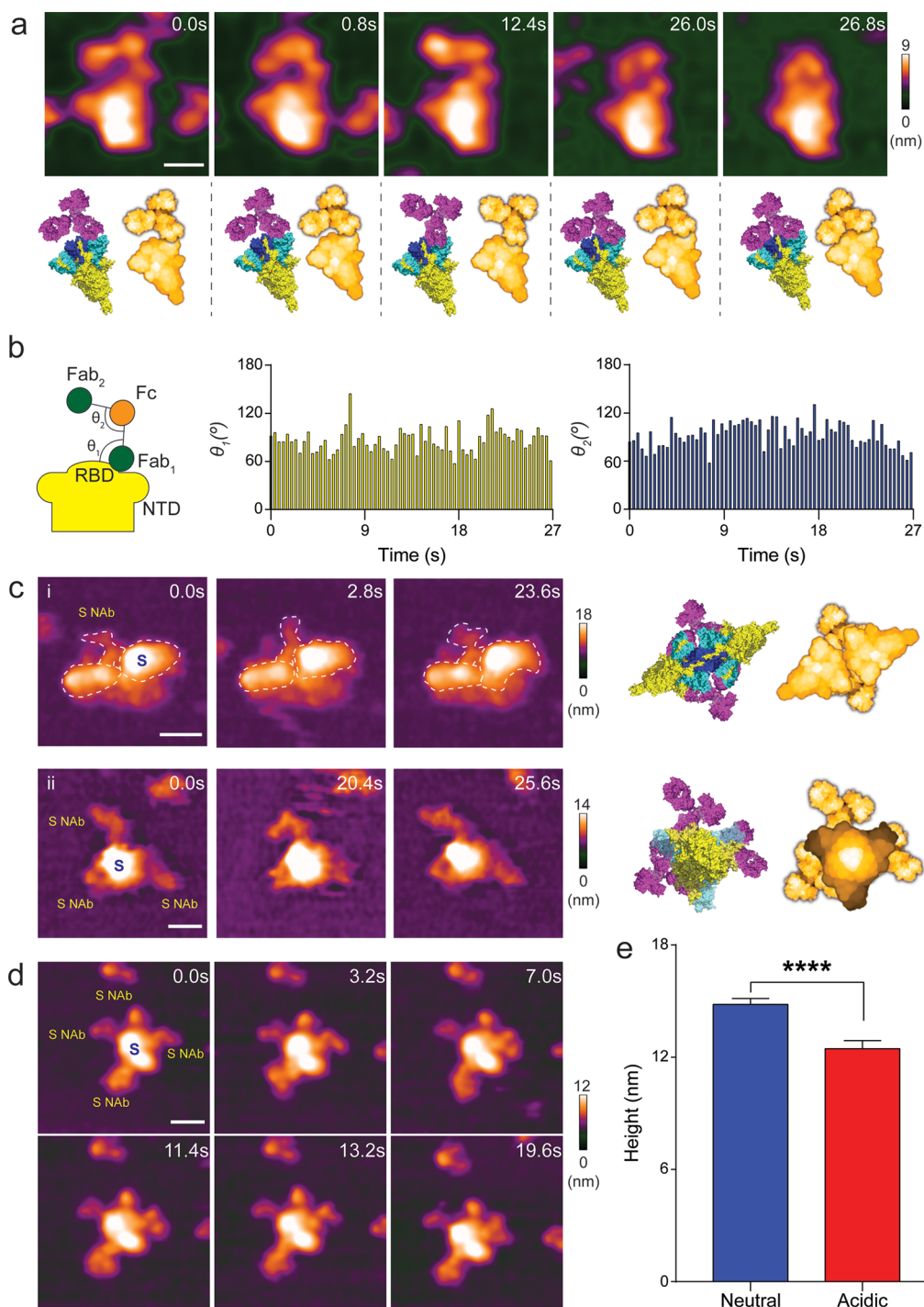
Figure 2. HS-AFM visualization of dynamic MM43−S protein interactions. (a) A representative set of HS-AFM image sequence illustrating the real-time binding of MM43 to the receptor-binding domain (RBD) of recombinant S protein. The molecular structure (PDB format) of IgG1 and S protein together with their respective simulated HS-AFM images are used to demonstrate the interaction orientations. These images are selected from Movie S4 ($n_{observation}$ = 4; scale bar: 25 nm). (b) Real-time angular changes (θ_1 and θ_2) during the MM43−S protein interaction. (c) Two representative HS-AFM image sequences demonstrating the nanotopology of the MM43−S protein immune complex. (c-i) shows bivalent binding of a single MM43 to two S proteins. (c-ii) shows an S protein trimer bound to three MM43. These images are extracted from Movie S5 ($n_{observation}$ = 10; scale bar: (c-i) 20 nm, (c-ii) 24 nm). (d) A representative set of HS-AFM image sequence indicating that acidification (pH 5) does not promote antibody shedding. These images are chosen from Movie S8a ($n_{observation}$ = 8; scale bar: 36 nm). (e) Significant reduction in the height of large immune complex after exposure to an acidic environment for 15 min. Data are presented as mean ± SEM ($n_{neutral}$ = 95, n_{acid} = 77; two-sided Mann−Whitney U test, ****p < 0.0001).

could be suitable for MM43 adsorption with optimal mobility. However, during HS-AFM scanning, we found that Ni²⁺-coated mica was better than bare mica for visualization of the Y conformation of MM43 (Figure 1d−f, Figure S1a, and Movie

S1). MM43 was loosely attached on bare mica in both flat/Y-shaped and lateral/T-shaped orientations (Figure S1b), and the lateral and flat orientations interchanged rapidly. In contrast, MM43 was strongly adsorbed on the poly-L-lysine
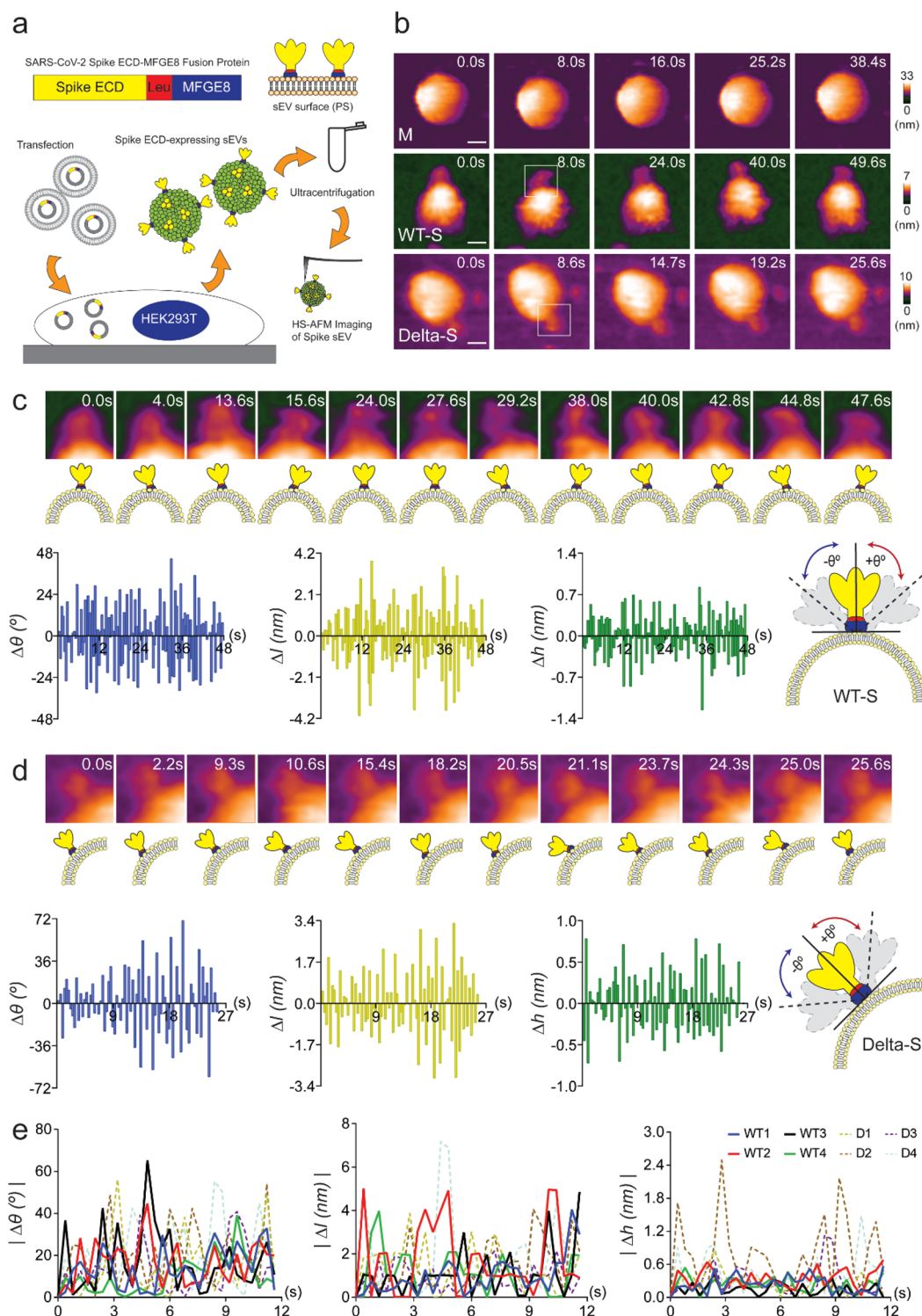
Figure 3. Nanotopology and structural dynamics of small extracellular vesicles (sEVs) expressing no S protein (mock; M), wild-type S protein (Wuhan-Hu-1; WT-S), or Delta variant S protein (Delta-S). (a) Schematic diagram showing the production of sEVs expressing S protein (S sEVs). An S−lactadherin fused protein is created by fusing an S ectodomain (ECD, yellow) and lactadherin (MFGE8, blue) with a leucine zipper (Leu, red). S−lactadherin fused protein and sEVs are synthesized by HEK293T cells, and then the fused proteins bind to phosphatidylserine (PS) in the sEV lipid bilayer to form S sEVs, which are purified using ultracentrifugation. S sEVs are then visualized using HS-AFM. (b) HS-AFM images illustrating a representative HS-AFM image sequence of M, WT-S, and Delta-S sEVs, respectively. S proteins (in white squares) are visible in WT-S and Delta-S sEVs. These images are selected from Movie S9 (n_M, n_{WT-S}, $n_{Delta-S}$ = 10; scale bars, M: 33 nm, WT-S: 12 nm, Delta-S: 10 nm). Representative structural dynamics of WT-S (c) or Delta-S (d) on S sEVs captured at high spatiotemporal resolution using HS-AFM (image size: 20 x 20 nm). These images are extracted from Movie S10. Real-time changes in tilting angle ($\Delta\theta$), length (Δl), and height (Δh) of S proteins were measured and are shown in bar graphs. (e) Comparison of real-time absolute values of $\Delta\theta$, Δl, and Δh indicating that both WT-S and Delta-S have comparable dynamic properties on sEV (n_{WT-S}, $n_{Delta-S}$ = 4).

(PLL)-coated mica (Figure S1c and Movie S2). The strong adsorption force stretched MM43 until the hinges connecting Fab and Fc regions were clearly visible (Figure S1c-1,2 and Movie S2a,b). Formalin-fixed MM43 consistently adopted the Y shape on the PLL-coated mica (Figure S1d). At high concentration, MM43 rapidly self-assembled (Figure S2a−d and Movie S3). This phenomenon usually occurs in the presence of antigens, at a high antibody concentration, or at a pH close to the antibody isoelectric point.[21,22] Self-assembly of IgG1 is mainly mediated by noncovalent Fab−Fab, Fc−Fc, and Fab−Fc bonds.[22] The hexameric ring topology of MM43 (Figure S2 and Movie S3) was consistent with that observed previously.[21,23] Therefore, we diluted MM43 to ensure it was predominantly monomeric. The cross-sectional height distribution of the MM43 was measured (Figure 1g) and yielded an average height of 3.47 nm ($n = 205$).

RBD-specific S NAbs are divided into four classes according to epitope location and epitope accessibility.[24] In contrast, the epitopes of NTD-specific S NAbs are rather confined in a particular site called the NTD supersite.[25] Several studies have reported that MM43 binds RBD to block SARS-CoV-2 infection.[26,27] Here, we intended to directly observe the binding pattern of MM43 to recombinant S protein (Wuhan-Hu-1 or wild type (WT)) under a physiological buffer. The results indicated that MM43 bound dynamically with the S protein (Figure 2a, Figure S3a,b, and Movies S4 and S5a,b). One Fab region (Fab$_1$) was firmly attached to the S protein, whereas another free Fab (Fab$_2$) and Fc regions were actively moving during HS-AFM imaging. The dynamic property of MM43 was depicted by measuring the angular changes in S protein−Fab$_1$−Fc (θ_1) and Fab$_1$−Fc−Fab$_2$ (θ_2) orientations as a function of time (Figure 2b). The flexibility of the antibody facilitates two Fab regions to actively search for epitopes. Preiner et al. depicted that IgGs could randomly walk with two "Fab feet" on surfaces of repeatedly spaced epitopes.[28] In the context of S protein, MM43 could bind either two RBDs of an S protein or two RBDs of two different S proteins. We found that a MM43 monomer interacted with two S proteins (Figure 2c-i and Movie S5c). Moreover, a single trimeric S protein often bound with three MM43 (Figure 2c-ii, Figure S3c, and Movie S5d,e). These findings imply that stable MM43 bivalent binding to two RBDs of a single S protein could be unfavorable even though a transient contact occurred during HS-AFM scanning (Figure 2a). Shaw and co-workers reported that the distance between two antigens could affect the bivalent binding affinity of all IgG subclasses.[29] According to their results, the bivalent binding affinity of IgGs is weak if two antigens are either too close (3−7 nm) or too far (17 nm and above).[29] The distance between two NTDs of a trimeric S protein is close to 80 Å or 8 nm,[30] and hence the distance between two RBDs should be shorter than that. These results explain why MM43 could not bind bivalently on a single S protein. According to our previous findings on the AFM topology of S protein in open and closed states,[13] our current results suggested that the MM43 and S protein interaction did not induce RBD opening. Moreover, S1 subunit shedding, an indicator of ADE,[8] did not occur after a trimeric S protein bound with three MM43. These findings suggested that MM43 could have a negligible risk of ADE.

Antibody-antigen interactions form large immune complexes (Figure S3d) including hexameric rings (Figure S3e) for phagocytosis (review in ref 31) and complement activation[32] to eliminate SARS-CoV-2. Nonetheless, certain S NAbs rather

enhance SARS-CoV-2 infectivity in FcγR-positive phagocytes after phagocytosis.[33] Like an endosome, acidification of a phagosome could promote antibody shedding,[34] and subsequently viral entry resumes. To elucidate the real-time acidification effect on the MM43−S protein interaction, we first scanned the immune complex under a neutral buffer (pH 7.4) then changed to an acidic buffer (pH 5). The result showed that a large immune complex was dissociated upon acidification (Figure S4a and Movie S6), as indicated by the rapid decrease in both height and color intensity and the increase in aggregate area (Figure S4b). Likewise, height reduction was also observed in large immune complexes after incubation in an acidic buffer for a period of time (Figure 2e). Zhou and co-workers reported that the S protein appears predominantly in the closed state at acidic pH to prevent antibody binding.[34] Nevertheless, the binding affinity of an antibody to RBD at acidic pH remained strong.[34] We noticed that acidification disrupted MM43 self-interaction (Figure S4c and Movie S7) but not the MM43−S protein interaction (Figure 2d Figure S4d-i,ii, and Movie S8a). These findings suggested that antibody shedding in an endosome or phagosome may not happen if neutralization of SARS-CoV-2 has occurred before endocytosis or phagocytosis. IgG1 self-assembly is dominantly mediated by electrostatic forces.[22] Upon acidification, both Fab and Fc regions become positively charged (Figure S4e) and repel each other, resulting in dissociation of MM43 oligomers (Figure S4c and Movie S7). Similarly, a recent study described that IgG1 antibodies are monomeric at acidic pH.[35] As was mentioned, IgG1 forms a hexameric ring in the presence of antigen.[21] Since the MM43 and S protein interaction was unperturbed by acidification, full or partial MM43-S protein hexameric rings were maintained (Figure S4d-iii,iv and Movie S8b−d).

Next, to mimic the dynamic interaction between S NAb and SARS-CoV-2, we first generated S protein expressing small extracellular vesicles (S sEV). We transfected HEK293T cells (Figure 3a) to produce sEVs expressing no S protein (mock; M), Wuhan-Hu-1 or wild-type S protein (WT-S), and Delta variant S protein (Delta-S). S protein ectodomain and lactadherin (*MFGE8*) were fused together with a leucine zipper. The C2 domain of lactadherin binds with high affinity to phosphatidylserine (PS), which allows the S−lactadherin fused protein to attach on the sEV surface. Although SARS-CoV-2[36,37] and S sEV have different surface protein compositions, the topologies of both entities are either spherical or ellipsoidal (Figure 3b, Figure S5a, and Movie S9). Furthermore, we were able to capture the lateral view of the S protein on sEVs (Figure 3b, Figure S5a, and Movie S9). However, its appearance was not enhanced by formalin fixation (Figure S5b and Movie S11). We previously reported that the dynamic behavior of recombinant S protein[13] resembles that on the viral surface.[38,39] Similarly, the S protein on sEV was actively tilting, extending, and retracting like a tentacle (Figure 3c,d and Movie S10). The changes in tilting angle, length, and height of S protein were comparable between WT-S and Delta-S sEVs (Figure 3e). A spatial analysis demonstrated that M sEVs had greater height and average diameter (AD) than WT-S and Delta-S sEVs (Figure S5c), but there was no large difference in height and AD between WT-S and Delta-S sEVs. The surface expression of S protein increased the surface roughness of sEVs (Figure S5d). Moreover, the surface roughness of Delta-S sEVs was significantly greater than that of WT-S sEVs. Wang and colleagues reported that spiky virus-
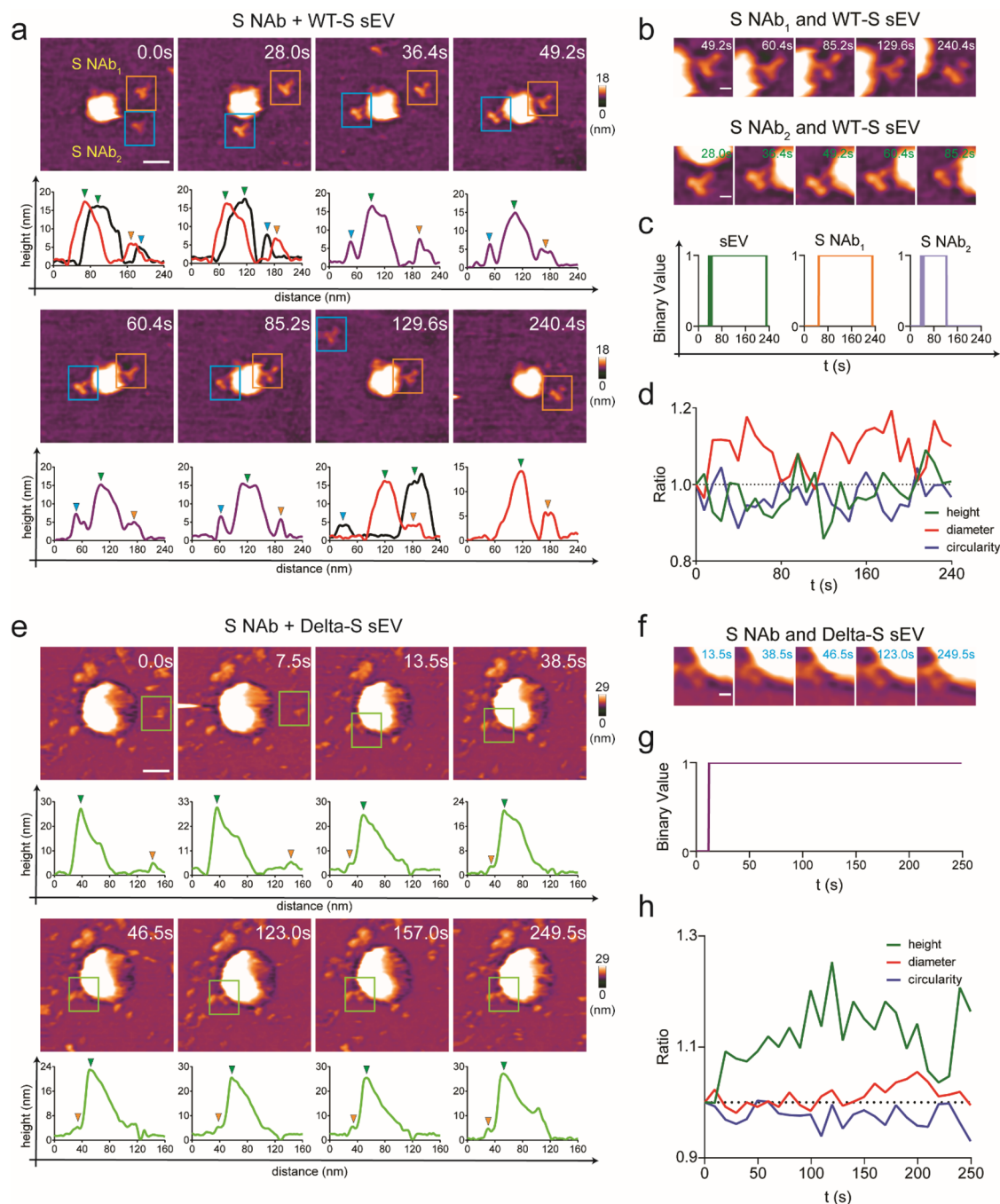
Figure 4. Real-time HS-AFM visualization of MM43 S NAb interactions with S sEVs. (a−d) A representative set of HS-AFM image sequence in (a) showing the approach and contact of two MM43 with one WT-S sEV. Graphs below the HS-AFM images plot the relative positions of two MM43 (S NAb$_1$ and S NAb$_2$) and the WT-S sEV at selected time points. The images are selected from Movie S12 ($n_{observation}$ = 5, scale bar: 60 nm; green triangle, WT-S sEV; orange triangle/box, S NAb$_1$; blue triangle/box, S NAb$_2$; orange line, WT-S sEV−S NAb$_1$ cross-sectional distance; black line, WT-S sEV−S NAb$_2$ cross-sectional distance; purple line, WT-S sEV−S NAb1−S NAb$_2$ cross-sectional distance). Magnified HS-AFM images in (b) show interactions of the WT-S sEV with S NAb$_1$ and S NAb$_2$ (scale bar: 16nm). Real-time contacts between MM43 and WT-S sEV are plotted in (c) as binary values (0, no contact; 1, contact). Real-time changes in the height, diameter, and circularity of the WT-S sEV are plotted in (d), relative to their respective values at t = 0. (e−h) A representative set of HS-AFM image sequence in (e) demonstrating the direct observation of a MM43−Delta-S sEV interaction. Graphs below the HS-AFM images in (e) plot the relative positions of the MM43 and Delta-S sEV at selected time points. These images are extracted from Movie S13 ($n_{observation}$ = 5, scale bar: 40 nm; green triangle, Delta-S sEV; orange triangle/green box, MM43). Magnified HS-AFM images in (f) show the MM43−Delta-S sEV interaction (scale bar: 8nm). Real-time contacts between the MM43 and Delta-S sEV are plotted in (g) as binary values (0: no contact; 1: contact). Real-time changes in the height, diameter, and circularity of the Delta-S sEV are plotted in (h), relative to their respective values at t = 0.

like nanoparticles with a rough surface showed remarkable cellular intake by HeLa cells.[40] This finding implies two important points. First, lactadherin conjugated on S sEV could bind the $\alpha v\beta 3$ or $\alpha v\beta 5$ integrin receptor of macrophages to induce phagocytosis (review in ref 41). Further study is needed to determine whether a rough surface improves the uptake of
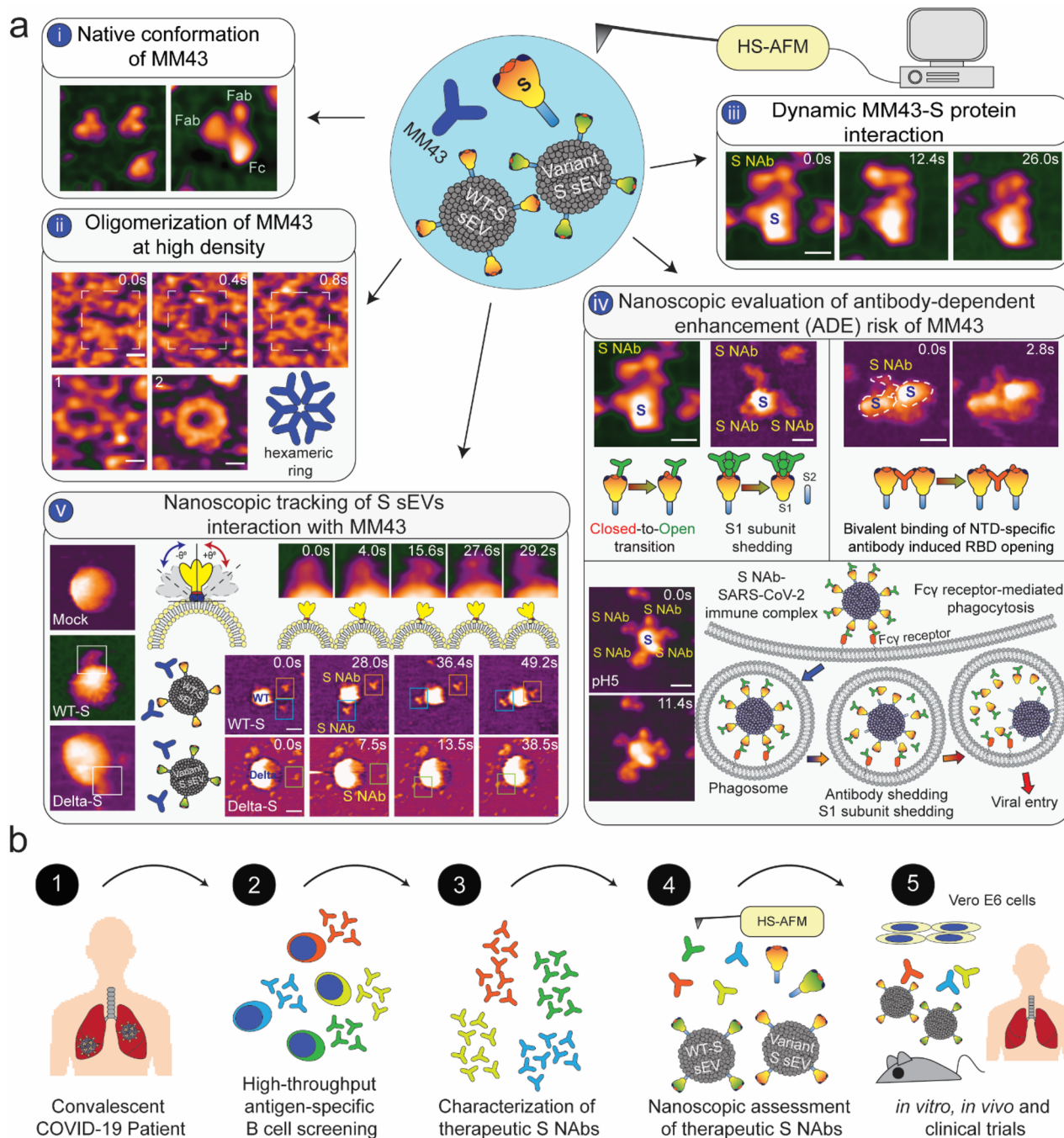
Figure 5. A nanoscopic perspective of S NAb and S protein interaction is essential for the assessment of S NAb therapeutic potential. (a) Nanoscopic observation of MM43 using HS-AFM reveals its native conformation (i) and intrinsic properties (ii), oligomerization for example. High spatiotemporal resolution enables HS-AFM to capture the dynamic MM43-S protein interaction and its binding pattern (iii). Direct visualization of S protein conformation in an immune complex at either neutral or acidic pH could provide important information related to antibody-dependent enhancement (ADE) such as RBD "Closed"-to-"Open" transition,[8,10] S1 subunit shedding,[8] and antibody shedding[34] (iv). S sEVs are safe alternative materials for nanoscopic tracking of the MM43 and SARS-CoV-2 interaction (v). Topology of S sEV and dynamic movement of S protein on sEV surface resemble SARS-CoV-2 virus. (b) Our results as summarized in (a) demonstrate that HS-AFM is feasible for nanoscopic assessment of potential therapeutic S NAbs. Patients recovered from COVID-19 have acquired immunity against SARS-CoV-2 (1). High-throughput screening of antigenic-specific B cells (2) is performed to isolate S NAbs for further evaluation of their therapeutic values (3). Nanoscopic assessment of these candidates using HS-AFM could provide essential information for better selection of S NAbs (4). Finally, the selected S NAbs will be used for downstream *in vitro* and *in vivo* experiments as well as clinical trials to validate their therapeutic efficacies (5).

Delta-S sEV by macrophages to boost host immunity against the variant. Second, viral surface roughness should be considered as an important physical property that enhances the infectivity of variants, including Delta. Zhang et al. stated the positive correlation between S protein density and SARS-

CoV-2 infection, in which the S protein density could reflect viral surface roughness.[42]

Mutations and deletions of amino acids in S protein confer immune escape to SARS-CoV-2 variants (reviewed in ref 3). Our real-time observations demonstrated that MM43

approached and contacted WT-S sEVs (Figure 4a–c and Movie S12) and Delta-S sEVs (Figure 4e–g and Movie S13). In addition, the MM43–S sEV interaction did not change the S sEV topology and spatial parameters (Figure 4d,h). In a premix setting, we found that MM43 firmly attached to both WT-S (Figure S6a and Movie S14c,d) and Delta-S sEVs (Figure S6a, and Movie S14e,f), but not to mock sEV (Figure S6a and Movie S14a,b). Moreover, some WT-S and Delta-S sEVs bound with multiple MM43 molecules (Figure S6b and Movie S15). Intriguingly, the tendency of multiple S NAb binding was only slightly lower in Delta-S sEV (18%) compared with that in WT-S sEV (25%) (Figure S6c and Table S1). Altogether, these findings suggested that MM43 could neutralize Delta variant S protein, consistent with other studies.[27]

In summary, we have developed a nanoscopic assessment technique to determine the binding pattern of S NAb, the S protein conformation in S NAb-S protein immune complex, the effect of endosomal or phagosomal pH on the S NAb-S protein interaction, and the dynamic interaction between S NAb and S sEVs (Figure 5a). These results are essential for the screening of appropriate S NAbs with a low risk of ADE to treat COVID-19. This approach is not limited to MM43 but is also practical for clinical-grade S Nabs (review in 17) and ADE-related anti-S protein antibodies.[8,10] Furthermore, in the near future, HS-AFM should be feasible to study anti-S protein monoclonal antibodies derived from both active and convalescent COVID-19 patients' sera to discover any possible new neutralizing antibodies against the variants, Omicron (B.1.1.529) for example, or new ADE mechanisms (Figure 5b).

■ ASSOCIATED CONTENT

ⓢ Supporting Information

The Supporting Information is available free of charge at https://pubs.acs.org/doi/10.1021/acs.nanolett.2c04270.

> Details on experimental methods, conformation of native and formalin-fixed MM43, oligomerization of MM43, dynamic interaction between MM43 and S protein, effect of acidification on MM43-S protein immune complex, conformation of native and formalin-fixed sEV expressing no S protein (mock), WT-S protein, and Delta-S protein, nanoscopic observation of MM43 interaction with mock sEV or S sEV), comparison of binding pattern of MM43 to WT-S sEV and Delta-S sEV, and movie captions (PDF)

> HS-AFM movie of the nanotopology of MM43 on nickel (Ni^{2+})-coated mica (MP4)

> HS-AFM movie of the nanotopology of single MM43 on poly-L-lysine-coated mica (MP4)

> HS-AFM movie of the real-time hexameric ring formation and stable hexameric rings formed at high density of MM43 (MP4)

> HS-AFM movie of the dynamic interaction between a MM43 and a recombinant S protein (MP4)

> HS-AFM movie of the different MM43–S protein interaction patterns (MP4)

> HS-AFM movie of the real-time dissociation of a large immune complex in response to acidification (MP4)

> HS-AFM movie of the real-time dissociation of a MM43 dimer in response to acidification (MP4)

> HS-AFM movie of the nanotopology of immune complex after incubated in an acidic environment (MP4)

> HS-AFM movie of the nanotopology of HEK293T-derived mock, WT-S, and Delta-S sEVs (MP4)

> HS-AFM movie of the real-time dynamic movements of WT-S and Delta-S on sEVs (MP4)

> HS-AFM movie of the nanotopology of formalin-fixed HEK293T-derived mock, WT-S, and Delta-S sEVs (MP4)

> HS-AFM movie of the real-time observation of MM43 interaction with WT-S sEVs (MP4)

> HS-AFM movie of the real-time observation of MM43 interaction with Delta-S sEVs (MP4)

> HS-AFM movie of the MM43 interaction with WT-S or Delta-S sEVs after 3 h incubation (MP4)

> HS-AFM movie of the multiple MM43 binding to WT-S or Delta-S sEVs (MP4)

■ AUTHOR INFORMATION

Corresponding Authors

Keesiang Lim — *WPI-Nano Life Science Institute, Kanazawa University, Kanazawa, Ishikawa 920-1192, Japan;* Email: limkeesiang@staff.kanazawa-u.ac.jp

Rikinari Hanayama — *WPI-Nano Life Science Institute, Kanazawa University, Kanazawa, Ishikawa 920-1192, Japan; Department of Immunology, Kanazawa University Graduate School of Medical Sciences, Kanazawa, Ishikawa 920-8640, Japan;* Email: hanayama@med.kanazawa-u.ac.jp

Richard W. Wong — *WPI-Nano Life Science Institute, Kanazawa University, Kanazawa, Ishikawa 920-1192, Japan; Cell-Bionomics Research Unit, Institute for Frontier Science Initiative (INFINITI), Kanazawa University, Kanazawa, Ishikawa 920-1192, Japan;* ⓘ orcid.org/0000-0002-2131-6595; Email: rwong@staff.kanazawa-u.ac.jp

Authors

Goro Nishide — *Division of Nano Life Science in the Graduate School of Frontier Science Initiative, WISE Program for Nano-Precision Medicine, Science and Technology, Kanazawa University, Kanazawa, Ishikawa 920-1192, Japan*

Elma Sakinatus Sajidah — *Division of Nano Life Science in the Graduate School of Frontier Science Initiative, Kanazawa University, Kanazawa, Ishikawa 920-1192, Japan*

Tomoyoshi Yamano — *WPI-Nano Life Science Institute, Kanazawa University, Kanazawa, Ishikawa 920-1192, Japan; Department of Immunology, Kanazawa University Graduate School of Medical Sciences, Kanazawa, Ishikawa 920-8640, Japan*

Yujia Qiu — *Division of Nano Life Science in the Graduate School of Frontier Science Initiative, Kanazawa University, Kanazawa, Ishikawa 920-1192, Japan*

Takeshi Yoshida — *Department of Immunology, Kanazawa University Graduate School of Medical Sciences, Kanazawa, Ishikawa 920-8640, Japan*

Akiko Kobayashi — *Cell-Bionomics Research Unit, Institute for Frontier Science Initiative (INFINITI), Kanazawa University, Kanazawa, Ishikawa 920-1192, Japan*

Masaharu Hazawa — *WPI-Nano Life Science Institute, Kanazawa University, Kanazawa, Ishikawa 920-1192, Japan; Cell-Bionomics Research Unit, Institute for Frontier*

Science Initiative (INFINITI), Kanazawa University, Kanazawa, Ishikawa 920-1192, Japan

Toshio Ando − *WPI-Nano Life Science Institute, Kanazawa University, Kanazawa, Ishikawa 920-1192, Japan;* orcid.org/0000-0001-8819-154X

Complete contact information is available at:
https://pubs.acs.org/10.1021/acs.nanolett.2c04270

Author Contributions

Conceptualization: K.L., R.W.W. Methodology: K.L., T.Y., T.A. Investigation: K.L., G.N., E.S.S., T.Y., Y.Q., T.Y. Visualization: K.L., G.N., E.S.S., Y.Q., A.K., M.H. Funding acquisition: K.L., R.H., R.W.W. Project administration: K.L., R.W.W. Supervision: K.L., R.W.W. Writing−original draft: K.L., R.W.W. Writing−review and editing: K.L., R.W.W. K.L., G.N., E.S.S., and T.Y. contributed equally.

Notes

The authors declare no competing financial interest.

■ REFERENCES

(1) World Health Organization. *Weekly epidemiological update on COVID-19*, 3 August 2022 (2022).

(2) Sajidah, E. S.; Lim, K.; Wong, R. W. How SARS-CoV-2 and Other Viruses Build an Invasion Route to Hijack the Host Nucleocytoplasmic Trafficking System. *Cells.* 2021, 10 (6), 1424.

(3) Jackson, C. B.; Farzan, M.; Chen, B.; Choe, H. Mechanisms of SARS-CoV-2 entry into cells. *Nat. Rev. Mol. Cell. Biol.* 2022, 23 (1), 3−20.

(4) Lopez Bernal, J.; Andrews, N.; Gower, C.; Gallagher, E.; Simmons, R.; Thelwall, S.; Stowe, J.; Tessier, E.; Groves, N.; Dabrera, G.; Myers, R.; Campbell, C. N. J.; Amirthalingam, G.; Edmunds, M.; Zambon, M.; Brown, K. E.; Hopkins, S.; Chand, M.; Ramsay, M. Effectiveness of Covid-19 Vaccines against the B.1.617.2 (Delta) Variant. *N. Engl. J. Med.* 2021, 385 (7), 585−594.

(5) Collier, A. Y.; Yu, J.; McMahan, K.; Liu, J.; Chandrashekar, A.; Maron, J. S.; Atyeo, C.; Martinez, D. R.; Ansel, J. L.; Aguayo, R.; Rowe, M.; Jacob-Dolan, C.; Sellers, D.; Barrett, J.; Ahmad, K.; Anioke, T.; VanWyk, H.; Gardner, S.; Powers, O.; Bondzie, E. A.; Wan, H.; Baric, R. S.; Alter, G.; Hacker, M. R.; Barouch, D. H. Differential Kinetics of Immune Responses Elicited by Covid-19 Vaccines. *N. Engl. J. Med.* 2021, 385 (21), 2010−12.

(6) Evans, J. P.; Zeng, C.; Carlin, C.; Lozanski, G.; Saif, L. J.; Oltz, E. M.; Gumina, R. J.; Liu, S.-L. Neutralizing antibody responses elicited by SARS-CoV-2 mRNA vaccination wane over time and are boosted by breakthrough infection. *Sci. Transl. Med.* 2022, 14 (637), No. eabn8057.

(7) Hwang, Y. C.; Lu, R. M.; Su, S. C.; Chiang, P. Y.; Ko, S. H.; Ke, F. Y.; Liang, K. H.; Hsieh, T. Y.; Wu, H. C. Monoclonal antibodies for COVID-19 therapy and SARS-CoV-2 detection. *J. Biomed Sci.* 2022, 29 (1), 1.

(8) Asarnow, D.; Wang, B.; Lee, W. H.; Hu, Y.; Huang, C. W.; Faust, B.; Ng, P. M. L.; Ngoh, E. Z. X.; Bohn, M.; Bulkley, D.; Pizzorno, A.; Ary, B.; Tan, H. C.; Lee, C. Y.; Minhat, R. A.; Terrier, O.; Soh, M. K.; Teo, F. J.; Yeap, Y. Y. C.; Seah, S. G. K.; Chan, C. E. Z.; Connelly, E.; Young, N. J.; Maurer-Stroh, S.; Renia, L.; Hanson, B. J.; Rosa-Calatrava, M.; Manglik, A.; Cheng, Y.; Craik, C. S.; Wang, C. I. Structural insight into SARS-CoV-2 neutralizing antibodies and modulation of syncytia. *Cell.* 2021, 184 (12), 3192−3204.

(9) Benton, D. J.; Wrobel, A. G.; Xu, P.; Roustan, C.; Martin, S. R.; Rosenthal, P. B.; Skehel, J. J.; Gamblin, S. J. Receptor binding and priming of the spike protein of SARS-CoV-2 for membrane fusion. *Nature.* 2020, 588 (7837), 327−330.

(10) Liu, Y.; Soh, W. T.; Kishikawa, J. I.; Hirose, M.; Nakayama, E. E.; Li, S.; Sasai, M.; Suzuki, T.; Tada, A.; Arakawa, A.; Matsuoka, S.; Akamatsu, K.; Matsuda, M.; Ono, C.; Torii, S.; Kishida, K.; Jin, H.; Nakai, W.; Arase, N.; Nakagawa, A.; Matsumoto, M.; Nakazaki, Y.; Shindo, Y.; Kohyama, M.; Tomii, K.; Ohmura, K.; Ohshima, S.; Okamoto, T.; Yamamoto, M.; Nakagami, H.; Matsuura, Y.; Nakagawa, A.; Kato, T.; Okada, M.; Standley, D. M.; Shioda, T.; Arase, H. An infectivity-enhancing site on the SARS-CoV-2 spike protein targeted by antibodies. *Cell.* 2021, 184 (13), 3452−3466.

(11) Lim, K. S.; Mohamed, M. S.; Wang, H.; Hartono; Hazawa, M.; Kobayashi, A.; Voon, D. C.; Kodera, N.; Ando, T.; Wong, R. W. Direct visualization of avian influenza H5N1 hemagglutinin precursor and its conformational change by high-speed atomic force microscopy. *Biochim. Biophys. Acta. Gen. Subj.* 2020, 1864 (2), 129313.

(12) Lim, K.; Kodera, N.; Wang, H.; Mohamed, M. S.; Hazawa, M.; Kobayashi, A.; Yoshida, T.; Hanayama, R.; Yano, S.; Ando, T.; Wong, R. W. High-Speed AFM Reveals Molecular Dynamics of Human Influenza A Hemagglutinin and Its Interaction with Exosomes. *Nano Lett.* 2020, 20 (9), 6320−28.

(13) Lim, K.; Nishide, G.; Yoshida, T.; Watanabe-Nakayama, T.; Kobayashi, A.; Hazawa, M.; Hanayama, R.; Ando, T.; Wong, R. W. Millisecond dynamic of SARS-CoV-2 spike and its interaction with ACE2 receptor and small extracellular vesicles. *J. Extracell. Vesicles.* 2021, 10 (14), No. e12170.

(14) Nishide, G.; Lim, K.; Mohamed, M. S.; Kobayashi, A.; Hazawa, M.; Watanabe-Nakayama, T.; Kodera, N.; Ando, T.; Wong, R. W. High-Speed Atomic Force Microscopy Reveals Spatiotemporal Dynamics of Histone Protein H2A Involution by DNA Inchworming. *J. Phys. Chem. Lett.* 2021, 12 (15), 3837−46.

(15) Mohamed, M. S.; Hazawa, M.; Kobayashi, A.; Guillaud, L.; Watanabe-Nakayama, T.; Nakayama, M.; Wang, H.; Kodera, N.; Oshima, M.; Ando, T.; Wong, R. W. Spatiotemporally tracking of nano-biofilaments inside the nuclear pore complex core. *Biomaterials.* 2020, 256, 120198.

(16) Mohamed, M. S.; Kobayashi, A.; Taoka, A.; Watanabe-Nakayama, T.; Kikuchi, Y.; Hazawa, M.; Minamoto, T.; Fukumori, Y.; Kodera, N.; Uchihashi, T.; Ando, T.; Wong, R. W. High-Speed Atomic Force Microscopy Reveals Loss of Nuclear Pore Resilience as a Dying Code in Colorectal Cancer Cells. *ACS Nano* 2017, 11 (6), 5567−78.

(17) Focosi, D.; McConnell, S.; Casadevall, A.; Cappello, E.; Valdiserra, G.; Tuccori, M. Monoclonal antibody therapies against SARS-CoV-2. *Lancet Infect Dis.* 2022, 22 (11), e311.

(18) Amyot, R.; Flechsig, H. BioAFMviewer: An interactive interface for simulated AFM scanning of biomolecular structures and dynamics. *PLoS Comput. Biol.* 2020, 16 (11), No. e1008444.

(19) Dolinsky, T. J.; Nielsen, J. E.; McCammon, J. A.; Baker, N. A. PDB2PQR: An automated pipeline for the setup of Poisson-Boltzmann electrostatics calculations. *Nucleic Acids Res.* 2004, 32 (Web server), W665.

(20) Baker, N. A.; Sept, D.; Joseph, S.; Holst, M. J.; McCammon, J. A. Electrostatics of nanosystems: application to microtubules and the ribosome. *Proc. Natl. Acad. Sci. U.S.A.* **2001**, *98* (18), 10037−41.

(21) Strasser, J.; de Jong, R. N.; Beurskens, F. J.; Wang, G.; Heck, A. J. R.; Schuurman, J.; Parren, P. W. H. I.; Hinterdorfer, P.; Preiner, J. Unraveling the Macromolecular Pathways of IgG Oligomerization and Complement Activation on Antigenic Surfaces. *Nano Lett.* **2019**, *19* (7), 4787−96.

(22) Arora, J.; Hu, Y.; Esfandiary, R.; Sathish, H. A.; Bishop, S. M.; Joshi, S. B.; Middaugh, C. R.; Volkin, D. B.; Weis, D. D. Charge-mediated Fab-Fc interactions in an IgG1 antibody induce reversible self-association, cluster formation, and elevated viscosity. *MAbs.* **2016**, *8* (8), 1561−74.

(23) Kominami, H.; Kobayashi, K.; Ido, S.; Kimiya, H.; Yamada, H. Immunoactivity of self-assembled antibodies investigated by atomic force microscopy. *RSC Adv.* **2018**, *8* (51), 29378−84.

(24) Barnes, C. O.; Jette, C. A.; Abernathy, M. E.; Dam, K. A.; Esswein, S. R.; Gristick, H. B.; Malyutin, A. G.; Sharaf, N. G.; Huey-Tubman, K. E.; Lee, Y. E.; Robbiani, D. F.; Nussenzweig, M. C.; West, A. P., Jr.; Bjorkman, P. J. SARS-CoV-2 neutralizing antibody structures inform therapeutic strategies. *Nature.* **2020**, *588* (7839), 682.

(25) Lok, S. M. An NTD supersite of attack. *Cell Host Microbe.* **2021**, *29* (5), 744−746.

(26) Dussupt, V.; Sankhala, R. S.; Mendez-Rivera, L.; Townsley, S. M.; Schmidt, F.; Wieczorek, L.; Lal, K. G.; Donofrio, G. C.; Tran, U.; Jackson, N. D.; Zaky, W. I.; Zemil, M.; Tritsch, S. R.; Chen, W. H.; Martinez, E. J.; Ahmed, A.; Choe, M.; Chang, W. C.; Hajduczki, A.; Jian, N.; Peterson, C. E.; Rees, P. A.; Rutkowska, M.; Slike, B. M.; Selverian, C. N.; Swafford, I.; Teng, I. T.; Thomas, P. V.; Zhou, T.; Smith, C. J.; Currier, J. R.; Kwong, P. D.; Rolland, M.; Davidson, E.; Doranz, B. J.; Mores, C. N.; Hatziioannou, T.; Reiley, W. W.; Bieniasz, P. D.; Paquin-Proulx, D.; Gromowski, G. D.; Polonis, V. R.; Michael, N. L.; Modjarrad, K.; Joyce, M. G.; Krebs, S. J. Low-dose in vivo protection and neutralization across SARS-CoV-2 variants by monoclonal antibody combinations. *Nat. Immunol.* **2021**, *22* (12), 1503−14.

(27) Syed, A. M.; Taha, T. Y.; Tabata, T.; Chen, I. P.; Ciling, A.; Khalid, M. M.; Sreekumar, B.; Chen, P. Y.; Hayashi, J. M.; Soczek, K. M.; Ott, M.; Doudna, J. A. Rapid assessment of SARS-CoV-2-evolved variants using virus-like particles. *Science.* **2021**, *374* (6575), 1626−32.

(28) Preiner, J.; Kodera, N.; Tang, J.; Ebner, A.; Brameshuber, M.; Blaas, D.; Gelbmann, N.; Gruber, H. J.; Ando, T.; Hinterdorfer, P. IgGs are made for walking on bacterial and viral surfaces. *Nat. Commun.* **2014**, *5*, 4394.

(29) Shaw, A.; Hoffecker, I. T.; Smyrlaki, I.; Rosa, J.; Grevys, A.; Bratlie, D.; Sandlie, I.; Michaelsen, T. E.; Andersen, J. T.; Högberg, B. Binding to nanopatterned antigens is dominated by the spatial tolerance of antibodies. *Nat. Nanotechnol.* **2019**, *14* (2), 184−190.

(30) Cerutti, G.; Guo, Y.; Liu, L.; Liu, L.; Zhang, Z.; Luo, Y.; Huang, Y.; Wang, H. H.; Ho, D. D.; Sheng, Z.; Shapiro, L. Cryo-EM structure of the SARS-CoV-2 Omicron spike. *Cell Rep.* **2022**, *38* (9), 110428.

(31) Stuart, L. M.; Ezekowitz, R. A. Phagocytosis: elegant complexity. *Immunity.* **2005**, *22* (5), 539−50.

(32) Wang, G.; de Jong, R. N.; van den Bremer, E. T.; Beurskens, F. J.; Labrijn, A. F.; Ugurlar, D.; Gros, P.; Schuurman, J.; Parren, P. W.; Heck, A. J. Molecular Basis of Assembly and Activation of Complement Component C1 in Complex with Immunoglobulin G1 and Antigen. *Mol. Cell* **2016**, *63* (1), 135.

(33) Li, D.; Edwards, R. J.; Manne, K.; Martinez, D. R.; Schafer, A.; Alam, S. M.; Wiehe, K.; Lu, X.; Parks, R.; Sutherland, L. L.; Oguin, T. H.; McDanal, C.; Perez, L. G.; Mansouri, K.; Gobeil, S. M.C.; Janowska, K.; Stalls, V.; Kopp, M.; Cai, F.; Lee, E.; Foulger, A.; Hernandez, G. E.; Sanzone, A.; Tilahun, K.; Jiang, C.; Tse, L. V.; Bock, K. W.; Minai, M.; Nagata, B. M.; Cronin, K.; Gee-Lai, V.; Deyton, M.; Barr, M.; Von Holle, T.; Macintyre, A. N.; Stover, E.; Feldman, J.; Hauser, B. M.; Caradonna, T. M.; Scobey, T. D.; Rountree, W.; Wang, Y.; Moody, M. A.; Cain, D. W.; DeMarco, C. T.; Denny, T. N.; Woods, C. W.; Petzold, E. W.; Schmidt, A. G.; Teng, I-T.; Zhou, T.; Kwong, P. D.; Mascola, J. R.; Graham, B. S.; Moore, I. N.; Seder, R.; Andersen, H.; Lewis, M. G.; Montefiori, D. C.; Sempowski, G. D.; Baric, R. S.; Acharya, P.; Haynes, B. F.; Saunders, K. O. In vitro and in vivo functions of SARS-CoV-2 infection-enhancing and neutralizing antibodies. *Cell.* **2021**, *184* (16), 4203.

(34) Zhou, T.; Tsybovsky, Y.; Gorman, J.; Rapp, M.; Cerutti, G.; Chuang, G. Y.; Katsamba, P. S.; Sampson, J. M.; Schön, A.; Bimela, J.; Boyington, J. C.; Nazzari, A.; Olia, A. S.; Shi, W.; Sastry, M.; Stephens, T.; Stuckey, J.; Teng, I. T.; Wang, P.; Wang, S.; Zhang, B.; Friesner, R. A.; Ho, D. D.; Mascola, J. R.; Shapiro, L.; Kwong, P. D. Cryo-EM Structures of SARS-CoV-2 Spike without and with ACE2 Reveal a pH-Dependent Switch to Mediate Endosomal Positioning of Receptor-Binding Domains. *Cell. Host. Microbe.* **2020**, *28* (6), 867−879.

(35) van Kampen, M. D.; Kuipers-De Wilt, L. H. A. M.; van Egmond, M. L.; Reinders-Blankert, P.; van den Bremer, E. T. J.; Wang, G.; Heck, A. J. R.; Parren, P. W. H. I.; Beurskens, F. J.; Schuurman, J.; de Jong, R. N. Biophysical Characterization and Stability of Modified IgG1 Antibodies with Different Hexamerization Propensities. *J. Pharm. Sci.* **2022**, *111* (6), 1587−1598.

(36) Kiss, B.; Kis, Z.; Pályi, B.; Kellermayer, M. S. Z. Topography, Spike Dynamics, and Nanomechanics of Individual Native SARS-CoV-2 Virions. *Nano Lett.* **2021**, *21* (6), 2675−80.

(37) Lyonnais, S.; Hénaut, M.; Neyret, A.; Merida, P.; Cazevieille, C.; Gros, N.; Chable-Bessia, C.; Muriaux, D. Atomic force microscopy analysis of native infectious and inactivated SARS-CoV-2 virions. *Sci. Rep.* **2021**, *11* (1), 11885.

(38) Ke, Z.; Oton, J.; Qu, K.; Cortese, M.; Zila, V.; McKeane, L.; Nakane, T.; Zivanov, J.; Neufeldt, C. J.; Cerikan, B.; Lu, J. M.; Peukes, J.; Xiong, X.; Kräusslich, H. G.; Scheres, S. H. W.; Bartenschlager, R.; Briggs, J. A. G. Structures and distributions of SARS-CoV-2 spike proteins on intact virions. *Nature.* **2020**, *588* (7838), 498−502.

(39) Turoňová, B.; Sikora, M.; Schürmann, C.; Hagen, W. J. H.; Welsch, S.; Blanc, F. E. C.; von Bülow, S.; Gecht, M.; Bagola, K.; Hörner, C.; van Zandbergen, G.; Landry, J.; de Azevedo, N. T. D.; Mosalaganti, S.; Schwarz, A.; Covino, R.; Mühlebach, M. D.; Hummer, G.; Krijnse Locker, J.; Beck, M. In situ structural analysis of SARS-CoV-2 spike reveals flexibility mediated by three hinges. *Science.* **2020**, *370* (6513), 203−8.

(40) Wang, W.; Wang, P.; Tang, X.; Elzatahry, A. A.; Wang, S.; Al-Dahyan, D.; Zhao, M.; Yao, C.; Hung, C. T.; Zhu, X.; Zhao, T.; Li, X.; Zhang, F.; Zhao, D. Facile Synthesis of Uniform Virus-like Mesoporous Silica Nanoparticles for Enhanced Cellular Internal-ization. *ACS Cent. Sci.* **2017**, *3* (8), 839−846.

(41) Lemke, G. How macrophages deal with death. *Nat. Rev. Immunol.* **2019**, *19* (9), 539−549.

(42) Zhang, L.; Jackson, C. B.; Mou, H.; Ojha, A.; Peng, H.; Quinlan, B. D.; Rangarajan, E. S.; Pan, A.; Vanderheiden, A.; Suthar, M. S.; Li, W.; Izard, T.; Rader, C.; Farzan, M.; Choe, H. SARS-CoV-2 spike-protein D614G mutation increases virion spike density and infectivity. *Nat. Commun.* **2020**, *11* (1), 6013.